High Resolution Metabolite Imaging in the Hippocampus Following Neonatal Exposure to the Environmental Toxin BMAA Using ToF-SIMS

N.B. When citing this work, cite the original published paper.

(article starts on next page)

High Resolution Metabolite Imaging in the Hippocampus Following Neonatal Exposure to the Environmental Toxin BMAA Using ToF-SIMS

Jörg Hanrieder,*[†,‡] Lorenz Gerber,[§] Åsa Persson Sandelius,[∥] Eva B. Brittebo,[⊥] Andrew G. Ewing,[†,‡,∥] and Oskar Karlsson[⊥,#]

[†]National Center for Imaging Mass Spectrometry, University of Gothenburg and Chalmers University of Technology, SE-412 96 Gothenburg, Sweden

[‡]Department of Chemical and Biological Engineering, Chalmers University of Technology, SE-412 96 Gothenburg Sweden

[§]Umeå Plant Science Centre, Department of Forest Genetics and Plant Physiology, Swedish University of Agricultural Sciences, SE-901 83 Umeå, Sweden

[∥]Department of Chemistry and Molecular Biology, University of Gothenburg, SE-412 96 Gothenburg, Sweden

[⊥]Department of Pharmaceutical Biosciences, Drug Safety and Toxicology, Uppsala University, SE-751 05 Uppsala, Sweden

[#]Department of Environmental Toxicology, Uppsala University, SE-751 05 Uppsala, Sweden

S *Supporting Information*

ABSTRACT: The environmental neurotoxin β-N-methylamino-L-alanine (BMAA) is suggested to be linked with neurodegenerative disease. In a rat model, neonatal exposure to BMAA induced selective uptake in the hippocampus and caused cell loss, mineralization and astrogliosis as well as learning and memory impairments in adulthood. Moreover, neonatal exposure resulted in increased protein ubiquitination in the cornus ammonis 1 (CA1) region of the adult hippocampus indicating that BMAA may induce protein aggregation. Time-of-flight secondary ion mass spectrometry (ToF-SIMS) based imaging is a powerful technology for spatial profiling of small molecular weight compounds in biological tissues with high chemical specificity and high spatial resolution. The aim of this study was to characterize neurochemical changes in the hippocampus of six month-old rats treated neonatally (postnatal days 9−10) with BMAA. Multivariate data analysis of whole section ToF-SIMS scans was performed to delineate anatomical regions of interest based on their chemical distribution pattern. Further analysis of spectral data obtained from the outlined anatomical regions, including CA1 and dentate gyrus (DG) revealed BMAA-induced long-term changes. Increased levels of phospholipids and protein fragments in the histopathologically altered CA1 region as well as phosphate depletion in the DG were observed. Moreover, high resolution SIMS imaging revealed a specific localization of phosphatidylcholine lipids, protein signals and potassium in the histopathologically altered CA1. These findings demonstrate that ToF-SIMS based imaging is a powerful approach for probing biochemical changes in situ and might serve as promising technique for investigating neurotoxin-induced brain pathology.
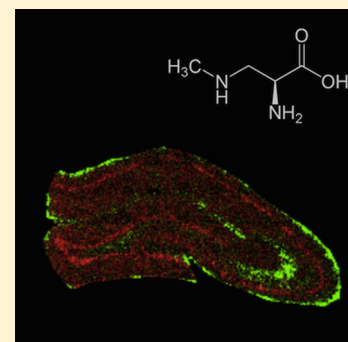
KEYWORDS: *Imaging mass spectrometry, beta-N-methylamino-L-alanine (BMAA), ALS/PDC, hippocampus, ToF-SIMS*

The environmental neurotoxin and nonprotein amino acid β-N-methylamino-L-alanine (BMAA) has received attention as a possible risk factor for neurodegenerative disease. Exposure to BMAA is suggested to be involved in the etiology of amyotrophic lateral sclerosis/parkinsonism-dementia complex (ALS/PDC) on the island of Guam[1,2] and has been detected in ALS and Alzheimer's disease patients in North America.[3] Both cyanobacteria and diatoms are reported to produce BMAA.[4,5] This neurotoxin has been detected in several water systems including temperate aquatic ecosystems and in mollusks and fish used for human consumption, indicating that BMAA might bioaccumulate in aquatic food chains.[6,7]

BMAA is suggested to induce neuronal degeneration via excitotoxic mechanisms although other mechanisms of toxicity may also be involved such as oxidative stress or misincorporation of the nonprotein beta-amino acid into protein.[8−10] The access of BMAA to the adult rodent brain is reported to be limited.[11,12] In contrast, our previous autoradiographic imaging revealed that ^{3}H-BMAA-derived radioactivity is transferred across the blood-brain barrier in neonatal mice, with a distinct localization in specific brain regions such as the hippocampus.[13] BMAA treatment of neonatal rats (PND; postnatal days 9−10) induced long-term cognitive impairments and changes in neuronal protein expression at adult age.[14−16] Neonatal

exposure resulted in progressive lesions in the hippocampus of adult rats including neuronal degeneration, cell loss, mineralization, astrogliosis, fibril formation, and increased protein ubiquitination.[17] In order to understand the mechanisms of BMAA-induced neurotoxicity following neonatal exposure more studies on the changes in the adult hippocampus are needed, as this brain area is essential for learning and memory.

A major objective when studying molecular mechanisms is the acquisition of molecular images for receiving spatial and temporal information on molecular abundance changes of endogenous compounds. Imaging mass spectrometry (IMS) has been demonstrated to be a valuable approach in biomedical research and represents a powerful technology for spatial profiling of lipids, neuropeptides and proteins in biological matrices.[18−20] In contrast to common molecular and histological techniques, IMS does not require any a priori knowledge of the potential target species. An integral advantage of time-of-flight secondary ion mass spectrometry (ToF-SIMS) based IMS is its high spatial resolution, often at the submicrometer scale (<500 nm), making it a powerful technology for spatial profiling of lipids and metabolites at a single cell level.[21] This is of particular relevance for studying complex and heterogeneous samples, such as neuronal tissues, which arguably constitute the most complex and least understood systems in the body.[22,23]

In the present study, we employed ToF-SIMS IMS to probe the distribution of small molecular weight compounds (<1000 Da), including lipids and metabolites, in the hippocampus of 6-month old rats with extensive BMAA-induced histopathological alterations (Figure 1). Multivariate statistical analysis tools were

Figure 1. Experimental design. Male pups were injected sc with BMAA or vehicle at PND 9−10 and evaluated in week 1−3 for acute behavioral impairments and in weeks 10−22 for long-term cognitive impairments. The animals were sacrificed at 6 months of age, and the excised brains were rapidly frozen and sectioned for ToF-SIMS analysis.

used for molecular histology-based dissection of anatomical regions and to identify hippocampal changes in endogenous metabolite profiles of BMAA-treated rats.

RESULTS AND DISCUSSION

ToF SIMS Imaging Elucidates Characteristic Lipid Localizations in the Hippocampus. For comprehensive analysis of the acquired IMS data, a two-step strategy based on multivariate analysis of image data and spectral data was applied. First, statistical analysis of image data by means of maximum autocorrelation factor (MAF) analysis was performed to outline anatomical regions of interest based on their biochemical identity.[24,25] This approach facilitated identification of major regions of the hippocampus including the CA regions as well as the DG (Figure 2). Moreover, a clear distinction from the adjacent white matter regions could be achieved. While the score (i.e., eigenvalue) images (Figure 2) illustrate the variance over the analyzed area for a specific factor, the biochemical information behind these differences is maintained in the loadings (eigenvectors). The variables with the most extreme loading value and therefore the largest impact

on the score-value, represent the most promising candidate compounds that show true localization to distinct regions of interest. In turn these species can serve as biochemical identifiers for a certain anatomical region. Indeed, manual inspection of single ion images revealed that characteristic localizations were observed for chemical species that displayed highest or lowest values in loading intensity (Figure 3). This included characteristic protein adducts (Na_2CN^+, $NaKCNO^+$, Figure 3A) that were found to be most prominent in the cell bodies of the CA regions as well as the granular cell layer (GCL) of the DG. Vitamin E (Figure 3A), fatty acids and cholesterol (Figure 3B) were in turn found to localize to the molecular layer of the DG as well as mossy fibers projecting from the DG to the CA3. Cholesterol and vitamin E are well-known constituents of the myelin sheathing surrounding the nerve fibers,[24] which further verifies the ability of SIMS imaging data to outline characteristic localizations of low molecular weight compounds in the brain.

Multivariate Spectral Analysis Identifies BMAA-Induced Long-Term Changes in Hippocampal Neurochemistry. To elucidate the mechanism of BMAA-induced long-term cognitive impairments[26] and neuropathological changes in adult rats following neonatal exposure, chemical changes in the hippocampus were studied using ToF-SIMS based imaging. OPLS-DA was performed for statistical comparison of the spectral data in order to examine chemical differences in an unbiased way between BMAA-treated animals and controls in the regions of hippocampus identified by the MAF analysis. All spectral data in both positive and negative ion mode were log2 normalized and merged for the respective regions generating a data matrix for each region (CA1 and DG) of 2007 individual mass values (variables) over all 6 animals (3 controls and 3 BMAA-exposed rats). Models for both CA1 and DG provided results that separated the controls from BMAA-treated animals and that explained large parts of the data sets variation (R2X cumulative DG: 0.86; CA1:0.53) (Figure 4B,C). The strong cross validation metrics (Q2 cumulative DG: 0.959; CA1:0.614) confirm the significance of the models.

Inspection of the corresponding loading values revealed that neonatal exposure to BMAA induced selective neurochemical changes in the adult hippocampus (SI Table 1 and 2). We have previously observed increased ubiquitination in the histopathologically altered CA1 region, suggesting that BMAA may induce protein misfolding and/or aggregation at this site.[14] In the present study, analysis of positive ion mode data revealed that major phosphatidylcholin (PC) lipid fragments (trimethylethylimine (TME) $M[C_5H_{12}N^+]$ 86.1) and the PC headgroup ($M[C_5H_{15}PO_4N^+]$ 184.1) were found to be increased in the CA1 of BMAA-exposed animals (Figure 5A). There was a distinct and striking colocalization between increased PC levels and the histopathologically altered regions of the CA1. The elevated PC level indicates accumulation of cell membranes and is most likely a result of inflammatory cell activation and recruitment. This is well in accordance with previously reported data on BMAA-induced astrogliosis observed in this area.[14]

In negative ion mode, inspection of the single ion images showed an increase of protein specific fragments ($M[CN^-]$ 26.01, $M[CNO^-]$ 42.01, $M[K_2CNO^+]$ 119.87) in the histologically altered CA1 region (Figure 5A). Increased protein content might be a consequence of gliosis in response to an initial neuronal damage but may also reflect a potential enrichment of protein aggregates in this region. Notably, recent ultrastructural examination of the affected CA1 region have
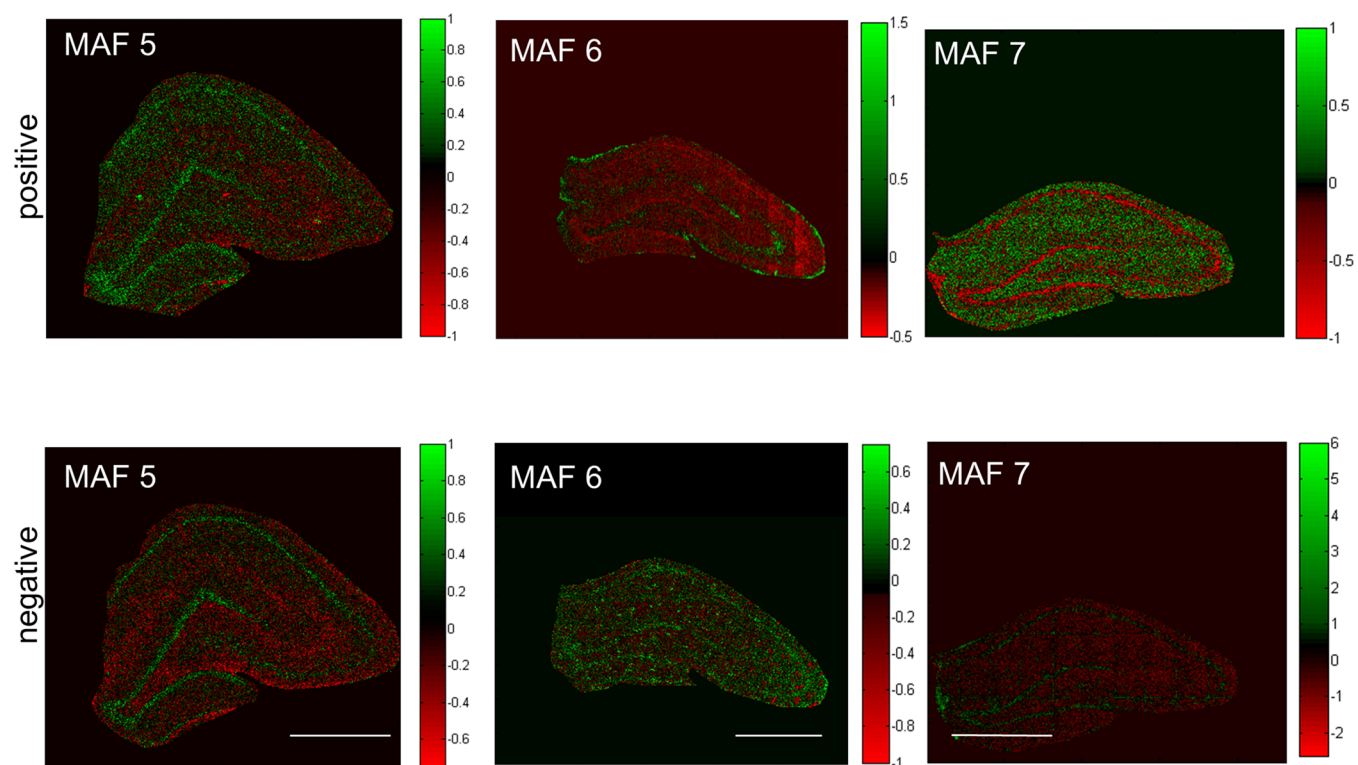
Figure 2. Multivariate image analysis for identification of anatomical regions of interest. ToF-SIMS imaging data of the hippocampus of 6-month old control animals ($n = 3$) were acquired in positive and negative ion mode and analyzed by means of maximum autocorrelation factor (MAF) analysis. The composition images depict individual scores (eigenvalues) for each pixel (spectrum) in the corresponding factors (MAF 3−5). The factors capture the variances over the tissue section and allow for an unbiased annotation of regions in the hippocampus based on chemical differences (scale bar = 1 mm).
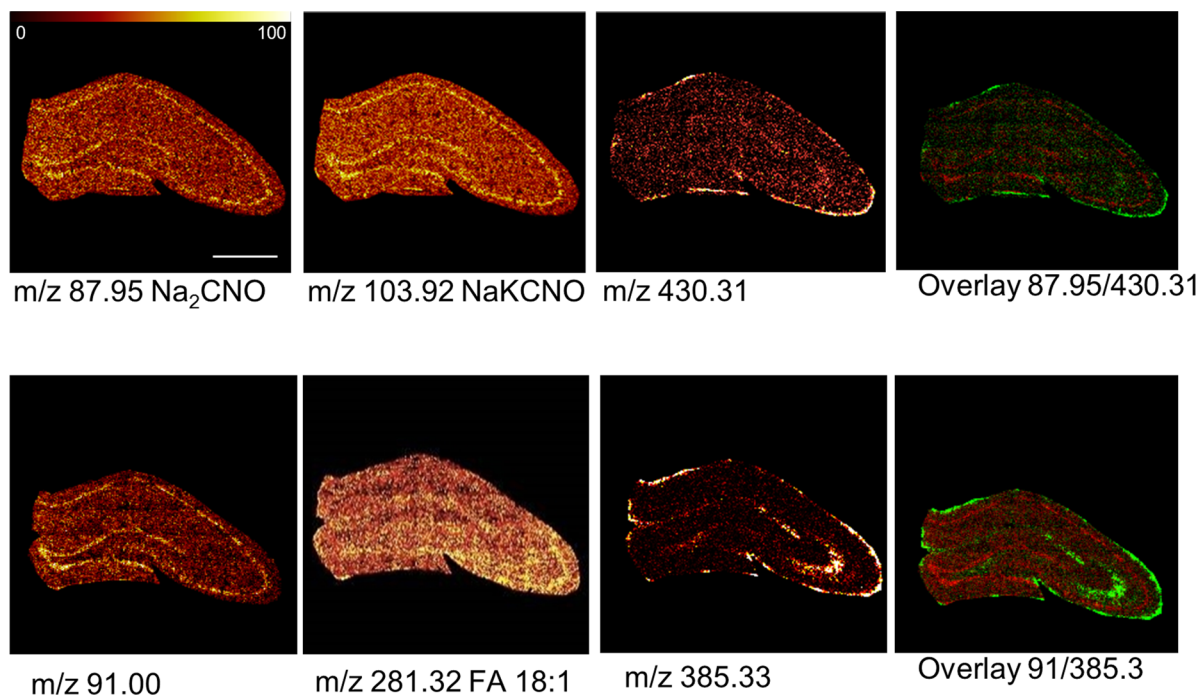

Figure 3. Single ion images of biochemical species that show region specific distributions. Positive and negative ion species show characteristic localization patterns that are well in line with anatomical regions of the hippocampus of 6-month old control animals. Protein specific fragments (pos: NaKCNO, Na$_2$CNO) were found in highest levels in the CA 1−4 and the granular cell layer of the DG. Similar observations were made for a yet unidentified species at m/z 91.00 in negative mode. Vitamin E (Vit.E, $[M + H]^+$ 430.31), fatty acids (FA 18:1, $[M − H]^-$ 281.32) and cholesterol (Chol., $[M − H]^-$ 385.33) were localized to the molecular layer of the DG as well as mossy fibers projecting from the DG to the CA3 (scale bar = 1 mm, color scale indicates relative intensity in %).
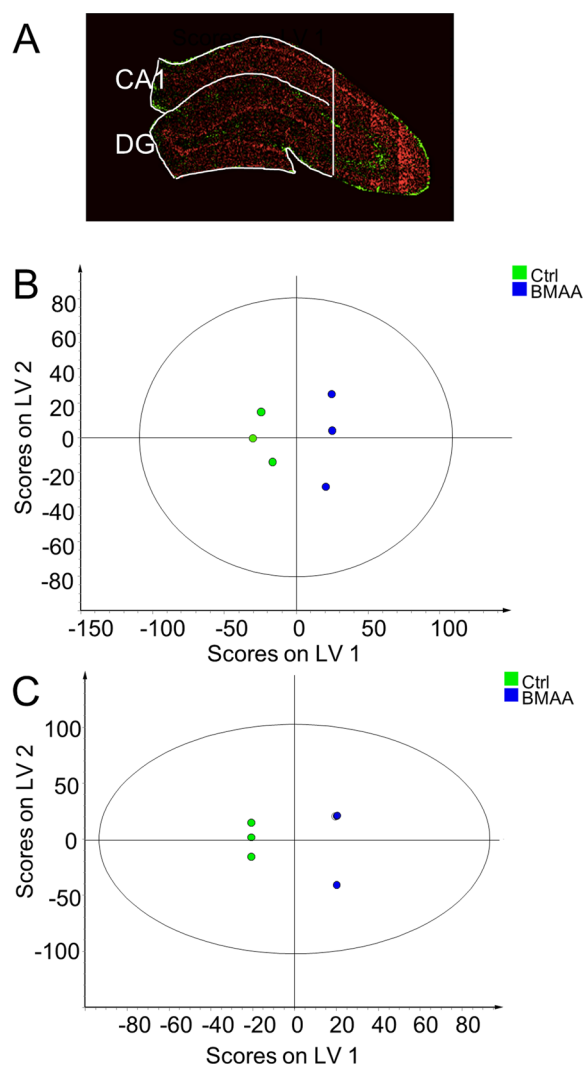
Figure 4. Multivariate analysis of spectral data reveals BMAA-induced hippocampal changes. MAF analysis was used to segment the hippocampal images into regions representing CA1 and DG (A). OPLS-DA models were calculated for both regions, clearly separating the control group from the BMAA group. (B) The analysis resulted in a 1 + 3 (1 predictive- + 3 orthogonal components) model for DG. The model explained 86% of the variation in the data set (R2X cumulative) with a predictive power of 0.96 (Q2 cumulative). (C) For the CA1, we obtained a 1 + 1 (1 predictive- + 3 orthogonal components) model, where 53% of the variation was explained with a predicative power of 0.61 (Q2 cumulative).

shown abundant bundles of closely packed intracellular parallel fibrils together with an enrichment of proteins that are known to form protein inclusions.[17]

Taken together, the present data demonstrate that there was a significant and selective increase of protein and lipid species in the histologically altered CA1 of BMAA-treated animals. This suggests that ToF-IMS IMS together with MAF analysis can be used to identify selective neurochemical changes in the brain. In addition, OPLS-DA revealed a significant decrease of phosphate ($M[PO_3^-]$ 78.97, $M[H_2PO_4^-]$ 96.98) in the granular layer of the DG in the BMAA-treated animals (Figure 5B). Phosphate serves as marker for DNA and a decrease of phosphate might therefore point to BMAA-induced reduction in cell division and proliferation in this region. An acute mild cell death (apoptosis) in DG has been reported in neonatal rats
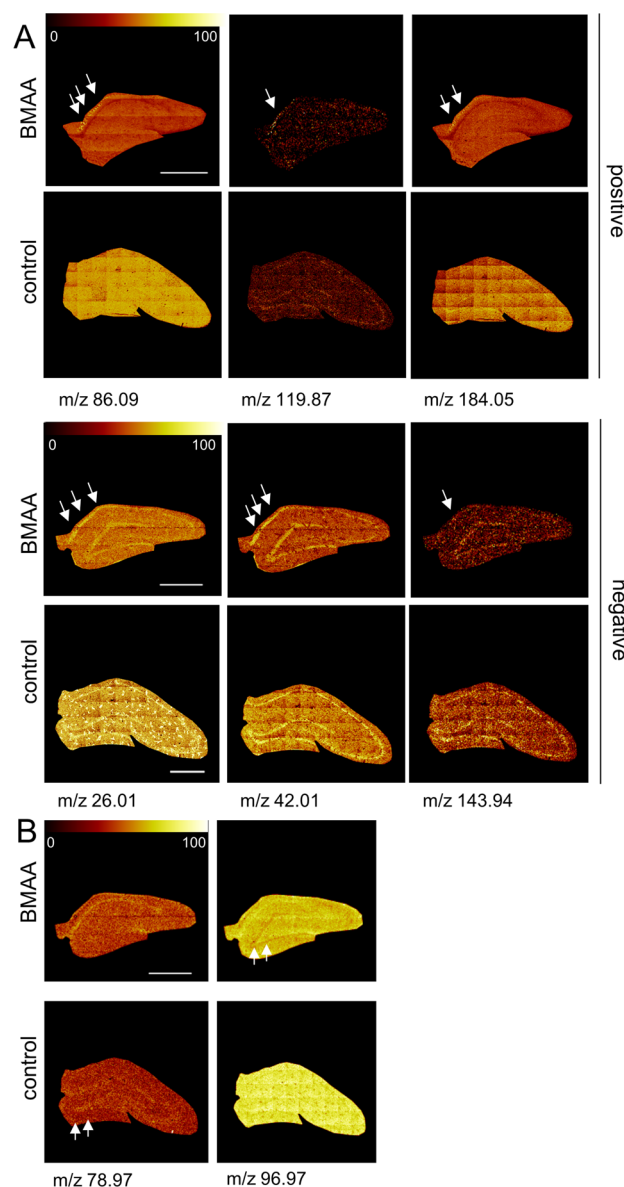

Figure 5. BMAA-induced changes of distinct molecular species in the hippocampus. Selective changes in the brain sections were identified in an unbiased way using multivariate analysis of spectral data. (A) In positive mode, the loadings reveal a significant increase of several mass peaks in the CA1 of BMMA-exposed animals compared to controls, including phospholipid fragments (TME, $M[C_5H_{12}N^+]$ 86.09; PC, $M[C_5H_{15}PNO_4^+]$ 184.05), and protein adduct ($M[K_2CNO^+]$ 119.87). (B) In negative mode, inspection of the imaging data show increase of protein associated signals ($M[CN^-]$ 26.01, $M[CNO^-]$ 42.00) as well as an unidentified peak, m/z 143.94 that were found to localize to the histopathologically altered CA1 region in the hippocampus (arrows) of BMAA animals compared to controls. (B) DG specific regulations comprised phosphate signals ($M[PO3^-]$ 79, $M[H2PO4^-]$ 97) that were found to be decreased in BMAA exposed animals compared to controls (scale bar = 1 mm; color scale indicates relative intensity in %).

exposed to BMAA.[27] Hence, it is possible that a BMAA-induced cell death in this region during the brain development may lead to a permanent neuronal cell loss. Moreover, the granular layer of the DG is a neurogenic zone expressing neuronal stem cells that may also be affected by neonatal BMAA exposure.
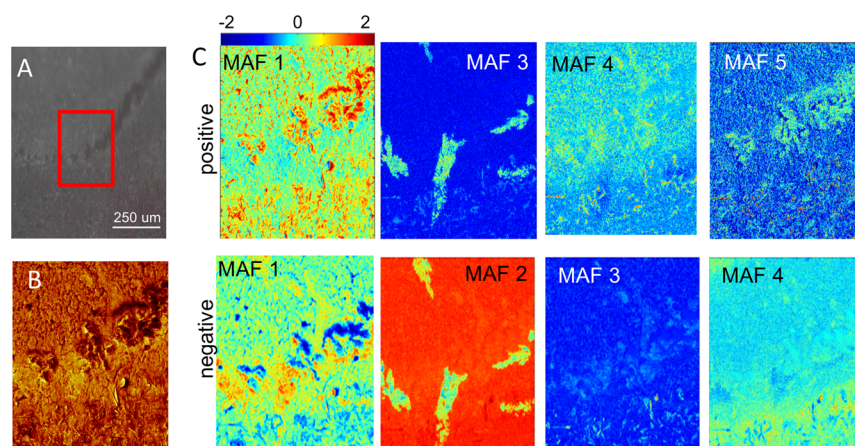
Figure 6. Burst alignment analysis of the BMAA-induced hippocampal changes. (A) Camera image showing the histopathologically altered region in the hippocampus of BMAA-treated rats. An area of 250 μm $\times$ 250 μm was analyzed by ToF-SIMS in burst-aligned mode (red square). (B) Total ion image of pos. ion mode image data for the analyzed region of interest (ROI). (C) MAF analysis of ROI data acquired in positive and negative ion mode showed chemical differences that allow for discrimination of the lesioned region based on the chemical composition as revealed by the corresponding loadings. The false color intensity represents the score (eigenvalue) for each pixel for different factors (i.e., MAF 1−5).
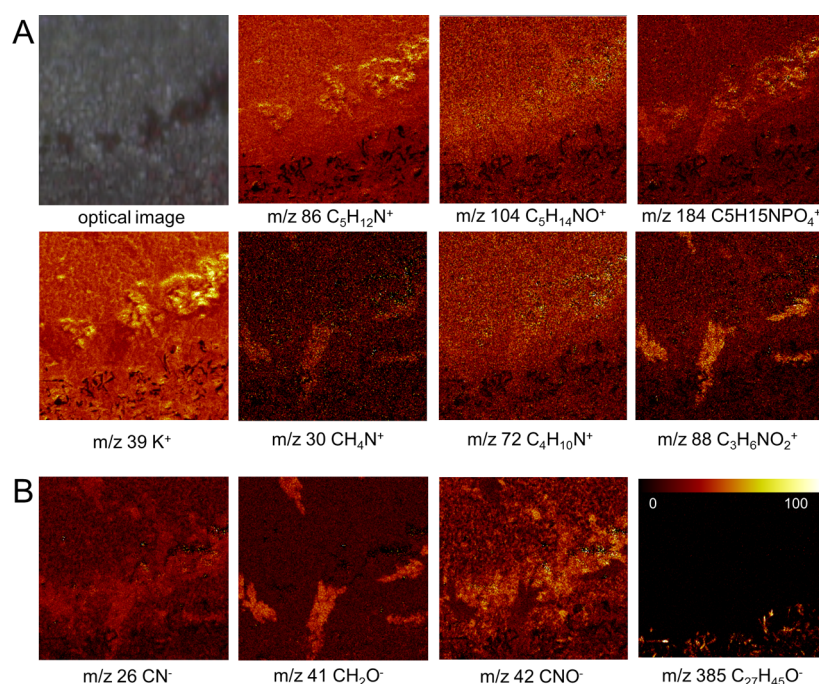

Figure 7. Single ion images of the BMAA-induced hippocampal changes. Manual inspection of variables (m/z) that showed the highest loading values in MAF based image analysis. (Camera image shows histopathological lesions observed in the CA1 region.) (A) In positive mode, the MAF data show phosphatidylcholine headgroup (PC, m/z 184) and its fragments (m/z 86 (TME, $C_5H_{12}N^+$), m/z 104 (choline, $C_5H_{14}NO^+$)) to be increased and localized to the CA1 in BMAA-treated rats, suggesting elevated phospholipid levels as a consequence of gliosis. Similarly, specific amino acid fragments (m/z 30, glycine; m/z 72, valine; m/z 88, aspartate) were increased at the BMAA-induced lesions in CA1 indicating protein increase, as a result of gliosis or protein aggregation. In addition, increased potassium (K^+) levels were observed that localize to the lesions. (B) Similar findings were observed for protein fragments (CN^-, C_2HO^-, CNO^-) in negative mode. Furthermore, elevated cholesterol levels were observed in the MAF loadings, which is a consequence of the adjacent white matter region (m/z 385). (Image size 250 $\times$ 250 μm; color scale indicates relative intensity in %.)

High Resolution Imaging to Probe the Histopathologically Altered Area in the Hippocampal CA1. To further study the BMAA-induced hippocampal lesions, ToF-SIMS experiments in burst-aligned mode were performed at <500 nm spatial resolution (Figure 6A, B). The imaging data were subjected to MAF analysis in order to reveal neurochemical localizations. The results demonstrated characteristic features that could be deconvoluted using multivariate analysis

and are encompassed in different factors (Figure 6C). Inspection of the corresponding loading data allowed us to deduce the chemical information associated with these features. PC fragments (m/z 86, m/z 104, Figure 7A) as well as protein (m/z 26, m/z 42, Figure 7B) and amino acid fragments (m/z 30, m/z 72, m/z 88, Figure 7A; m/z 41 Figure 7B) were found to colocalize with the BMAA-induced lesion in CA1, similar to the findings from whole tissue imaging. This further validates

the hypothesis that phospholipid and protein increase are associated with BMAA-induced neuropathology.

Finally, MAF analysis revealed an accumulation of potassium (K^+) associated with the lesions in the CA1 of BMAA-treated animals (Figure 7A). Rapid increase in extracellular K^+ concentration occurs in many CNS conditions including ischemia, traumatic brain injury, and epileptic seizures.[28] The observed K+ distribution appears to be diffuse, which corresponds to the pattern of GFAP expression as observed with immunohistochemistry (Figure 8) pointing toward
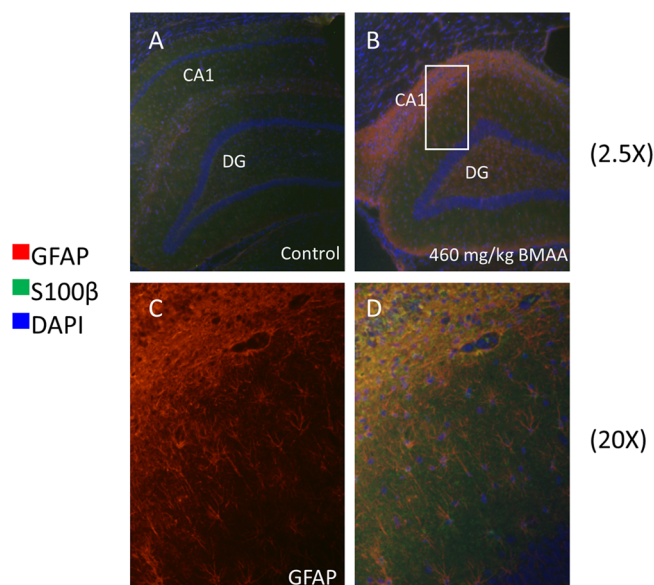
GFAP
S100β
DAPI

Figure 8. Immunohistochemistry of hippocampus. Double antigen staining was performed against GFAP and S100 beta on hippocampal sections of control (A) and BMAA exposed animals (B). The data show massive gliosis and reactive astrocyte species localizing to the histopathologically altered region in the hippocampus of BMAA-treated rats. This was indicated by increased GFAP immune-reactivity (red) in the CA1 of BMAA exposed animals (B−D) compared to controls (A). (C) Magnification of outlined area indicated in (B). GFAP positive cells (C) were also found to stain positively for S100 beta serving as additional marker for astrocyte activation (B,D). Magnifications: (A,B) lens × 10; (C,D) lens × 20.

BMAA-induced astrogliosis. Indeed, high extracellular K^+ concentrations can evoke changes in astrocyte morphology and GFAP expression.[28] Upon K^+ efflux as a result of neuronal damage, astrocytes initially exert a neuroprotective role via K^+ uptake in an effort to maintain K^+ homeostasis in CNS, which ultimately leads to astrogliosis.[28] The observed increase in K^+ might therefore be a consequence of neuronal cell death and partially be responsible for the initiation of astrogliosis in the BMAA-treated rats.

Immunohistochemistry Validates BMAA-Induced Gliosis. The increase in phospholipid and protein signals observed in the hippocampal CA1 could be a result of increased cell numbers in this region or increased activity of residing cells. Previous studies have demonstrated increased astrogliosis in this area in the hippocampus of adult rats treated neonatally with BMAA.[14,27] Increased glial fibrillary acidic protein (GFAP) and S100β levels can serve as a marker for brain damage and astrogliosis. Hence, to further validate the presence of astrogliosis, immunohistochemistry (IHC) was used to visualize astrocytic activity by GFAP and S100β expression in the hippocampus of control and BMAA exposed animals (Figure 8). Immunolabeling of GFAP and S100β revealed a marked upregulation of the proteins confirming an ongoing massive astrogliosis in the CA1 region of BMAA-exposed animals.

Astrocytes are important local regulators of neuroprotective innate inflammatory responses. Activation of astrocytes is accompanied by the secretion of soluble mediators, such as CXCL10, CCL2, and interleukin-6.[29] These mediators can initiate different types of events, including activation of neighboring cells and further amplification of local innate immune response as well as recruitment of blood immune cells. The balance between astrocyte mediated inflammatory and immunosuppressive pathways is fundamental for controlled reactions to CNS trauma and dysregulation of these pathways can lead to neurodegeneration.[29]

Taken together, the IHC data further support the ToF-SIMS observations in that astroglial migration and activation contribute to increased lipid and protein signal in the CA1 upon neonatal BMAA exposure. PC lipids may therefore serve as a marker for neuroglial cell activation and immune response in BMAA-induced brain damage.

CONCLUSIONS

The present study demonstrates the potential of ToF-SIMS IMS as a promising technique for spatial studies of small molecular weight compounds changes underlying neurotoxin-induced brain pathology. Using an unbiased segmentation approach the technique was used to elucidate locally confined changes in the CA1 and DG in the hippocampus of adult rats neonatally exposed to the environmental neurotoxin BMAA.

METHODS

Chemicals and Reagents. β-N-Methylamino-L-alanine (L-BMAA) hydrochloride (≥97%) was obtained from Sigma-Aldrich (St. Louis, MO). TissueTek optimal cutting tool (OCT) was purchased from Sakura Finetek (AJ Alphen aan den Rijn,The Netherlands). All chemicals were of pro-analysis grade and purchased from Sigma-Aldrich. Water was purified with a Milli-Q (Millipore, Bedford, MA) purification system.

Experimental Design. Pregnant outbred Wistar rats were obtained and gave birth to full-term offspring. Male pups were given one daily sc injection (20 μL/g) of 460 mg/kg (corresponding to 600 mg/kg BMAA·HCl; $n = 3$) freshly dissolved in Hanks' balanced salt solution, or vehicle ($n = 3$), for 2 days on PND 9−10. All animal experiments were approved by the Uppsala Ethical Committee on Animal Experiments and followed the guidelines of Swedish legislation on animal experimentation (Animal Welfare Act SFS1998:56) and European Union legislation (Convention ETS123 and Directive 86/609/EEC). The BMAA-induced short- and long-term behavioral effects as well as the histopathological changes have been published separately[14] (Figure 1).

Sample Preparation. The animals were sacrificed by decapitation at 6 month of age, the brains were excised and quickly frozen in dry ice followed by storage at −80 °C. Coronal cryosections were obtained from the right hemisphere of all animals at the level of hippocampus (−3.36 mm relative to the bregma).[30] The brain sections (12 μm) were thaw mounted on conductive glass slides (indium tin oxide, ITO, Bruker Daltonics, Bremen, Germany), dried under vacuum for 10 min, and stored at −80 °C until further use.

ToF-SIMS Analysis. An ION-TOF V ToF-SIMS instrument (IONTOF GmbH, Münster, Germany) equipped with a Bi_3^+ cluster ion gun as primary ion source was used for SIMS imaging. For whole section analysis, data were acquired in high current bunched mode[31] with a pulsed primary ion current of 0.25 pA at 25 keV and a maximum ion dose density was 1.5×10^9 ions/cm². Scans were acquired using the stage "scan macro raster function" with 10 shots per

pixel on 0.4 mm × 0.4 mm areas (patches) with 200 measurements per millimeter, resulting in a pixel resolution of 5 μm. This acquisition mode comprises stepwise acquisition of the 0.4 × 0.4 mm^2 patches. Each patch is acquired in electrostatic raster mode where the beam is moved over the field of view. The whole tissue area is analyzed by stepwise acquisition of these patches as achieved by stepwise movement of the sample stage. Both positive and negative ion mode data were collected. High resolution images of CA1 reqion were collected in burst-alignment mode[31] with a pulsed primary ion current of 0.04 pA at 25 keV and an ion dose of 8.8×10^{11} ions/cm^2. Fifty scans were acquired from a predefined quadratic scan area with 250 μm in edge length. Images comprising 512 × 512 pixels were acquired resulting in a spatial resolution of 488 nm. The mass resolution in high current bunch mode was about $M/\Delta M = 5 \times 10^3$. Conversely, burst-alignment mode mass resolution was $M/\Delta M = 350$ fwhm at m/z 500. Therefore, m/z values are specified with two digits in bunched mode and given as absolute values for burst aligned experiments.

Raw Data Processing. All spectra were acquired and processed with the Surface Lab software (v. 6.3 ION-TOF). All spectra were calibrated internally to signals of $[C]^+$, $[CH]^+$, $[CH_2]^+$, $[CH_3]^+$, $[C_5H_{15}PNO_4]^+$, and $[C_{27}H_{45}]^+$ were used as calibration points in positive mode and $[C]^-$, $[CH]^-$, $[CH_2]^-$, $[O]^-$, $[C_{16}H_{31}O_2]^-$, and $[C_{18}H_{35}O_2]^-$ in negative ion mode. Two mass interval lists were created (one for each ion polarity) which contained the list of m/z values to be included in the multivariate analysis. Mass interval lists were created by peak search of all individual samples according to the following search parameters: $S/N > 3$, width 0.8 Da. The assigned mass peaks were collected in the same mass interval list and redundant peak assignments removed.

Data Analysis. For image analysis of whole tissue scans and burst alignment data, the whole imaging data set was exported as *bif6* file and subjected to multivariate analysis by means of maximum autocorrelation factor analysis using plstoolbox (eigenvector Research Inc., Wenatchee, WA) in Matlab (R2012a, MathWorks, Natick, MA). For multivariate data analysis of spectral data, anatomical regions of the hippocampus were assigned using the implemented ROI feature. The dentate gyrus (DG) as well as the cornus ammonis region 1 (CA1) were assigned and reconstructed with the respective mass list (pos/neg ion mode) using the Mass Explorer of the Surface Lab Software (v 6.1, IONTOF). Peak area values for all ROI and animals, respectively, were evaluated by applying the multivariate data analysis method Orthogonal Projection to Latent Structures by Partial Least Squares—Discriminant Analysis (OPLS-DA)[32] using SIMCA (version 13.0, Umetrics, Umeå, Sweden). OPLS-DA uses group information coded in a binary matrix Y to decompose the X matrix into between-class and within-class variation. The OPLS-DA model effectively separates the discriminatory direction in the predictive scores from the within-group (orthogonal) scores, making the corresponding predictive loading vector straightforward to interpret. The predictive component loading also provides a direct measure of the influence of each variable. Further analysis of single lipid peaks and comparisons between groups was performed with two-tailed paired t test at a 95% confidence interval. Identification of mass peaks was done using tentative assignment by comparing the accurate mass to previously reported values in the literature[21] as well as matching of isotopic distribution.

Immunohistochemistry. Double-antigen fluorescent immunohistochemistry (IHC) was performed on brain sections from selected BMAA-treated and control animals using rabbit anti-S100-β (1:200, Abcam, Cambridge, U.K.) in combination with mouse anti-GFAP (1:500, Millipore, Temecula, CA) as primary antibodies. The fluorescent secondary antibodies anti-rabbit Alexa Fluor 488 (1:200, Invitrogen, Carlsbad, CA) and anti-mouse Alexa Fluor 555 (1:200, Invitrogen, Carlsbad, CA) were used for visualization. Cell nuclei were stained with DAPI (4,6-diamidino-2-phenylindole). Sections incubated without primary antibody (only the antibody diluent, 2.5% horse serum in phosphate buffered saline, in the primary antibody step) served as negative controls.

■ ASSOCIATED CONTENT

ⓢ Supporting Information

SI Tables 1 and 2, and SI Figures 1−4. This material is available free of charge via the Internet at http://pubs.acs.org.

■ AUTHOR INFORMATION

Corresponding Author

*Mailing address: Department of Chemical and Biological Engineering, Chalmers University of Technology, Kemivägen 10, SE-41296 Gothenburg, Sweden. E-mail: jorg.hanrieder@ chalmers.se. Phone: (+46) 31 7723050.

Author Contributions

The study was conceived and designed by J.H. Experiments were performed by J.H. and O.K. Data were analyzed and discussed by J.H., L.G., Å.S.P., E.B., A.G.E., and O.K. Manuscript was written by J.H., L.G., Å.S.P., E.B., A.G.E., and O.K.

Notes

The authors declare no competing financial interest.

■ ACKNOWLEDGMENTS

■ ABBREVIATIONS

IMS, imaging mass spectrometry; BMAA, beta-*N*-methylamino-L-alanine; MALDI, matrix assisted laser desorption/ionization mass spectrometry; MAF, maximum autocorrelation factor; PC, phosphatidylcholine; GFAP, glial fibrillary acidic protein

■ REFERENCES

(1) Banack, S. A., and Cox, P. A. (2003) Biomagnification of cycad neurotoxins in flying foxes: implications for ALS-PDC in Guam. *Neurology 61*, 387−389.

(2) Spencer, P. S., Nunn, P. B., Hugon, J., Ludolph, A. C., Ross, S. M., Roy, D. N., and Robertson, R. C. (1987) Guam amyotrophic lateral sclerosis-parkinsonism-dementia linked to a plant excitant neurotoxin. *Science 237*, 517−522.

(3) Pablo, J., Banack, S. A., Cox, P. A., Johnson, T. E., Papapetropoulos, S., Bradley, W. G., Buck, A., and Mash, D. C. (2009) Cyanobacterial neurotoxin BMAA in ALS and Alzheimer's disease. *Acta Neurol. Scand.*, 216−225.

(4) Cox, P. A., Banack, S. A., Murch, S. J., Rasmussen, U., Tien, G., Bidigare, R. R., Metcalf, J. S., Morrison, L. F., Codd, G. A., and Bergman, B. (2005) Diverse taxa of cyanobacteria produce beta-*N*-methylamino-L-alanine, a neurotoxic amino acid. *Proc. Natl. Acad. Sci. U.S.A. 102*, 5074−5078.

(5) Jiang, L., Eriksson, J., Lage, S., Jonasson, S., Shams, S., Mehine, M., Ilag, L. L., and Rasmussen, U. (2014) Diatoms: A Novel Source for the Neurotoxin BMAA in Aquatic Environments. *PLoS One 9*, e84578.

(6) Jonasson, S., Eriksson, J., Berntzon, L., Spacil, Z., Ilag, L. L., Ronnevi, L. O., Rasmussen, U., and Bergman, B. (2010) Transfer of a cyanobacterial neurotoxin within a temperate aquatic ecosystem suggests pathways for human exposure. *Proc. Natl. Acad. Sci. U.S.A. 107*, 9252−9257.

(7) Brand, L. E., Pablo, J., Compton, A., Hammerschlag, N., and Mash, D. C. (2010) Cyanobacterial Blooms and the Occurrence of the

neurotoxin beta-*N*-methylamino-L-alanine (BMAA) in South Florida Aquatic Food Webs. *Harmful Algae 9*, 620–635.

(8) Copani, A., Canonico, P. L., Catania, M. V., Aronica, E., Bruno, V., Ratti, E., van Amsterdam, F. T., Gaviraghi, G., and Nicoletti, F. (1991) Interaction between beta-N-methylamino-L-alanine and excitatory amino acid receptors in brain slices and neuronal cultures. *Brain Res. 558*, 79–86.

(9) Rao, S. D., Banack, S. A., Cox, P. A., and Weiss, J. H. (2006) BMAA selectively injures motor neurons via AMPA/kainate receptor activation. *Exp. Neurol. 201*, 244–252.

(10) Karlsson, O., Jiang, L., Andersson, M., Ilag, L. L., and Brittebo, E. B. (2014) Protein association of the neurotoxin and non-protein amino acid BMAA (beta-*N*-methylamino-L-alanine) in the liver and brain following neonatal administration in rats. *Toxicol. Lett. 226*, 1–5.

(11) Smith, Q. R., Nagura, H., Takada, Y., and Duncan, M. W. (1992) Facilitated transport of the neurotoxin, beta-*N*-methylamino-L-alanine, across the blood-brain barrier. *J. Neurochem. 58*, 1330–1337.

(12) Karlsson, O., Berg, C., Brittebo, E. B., and Lindquist, N. G. (2009) Retention of the cyanobacterial neurotoxin beta-*N*-methyl-amino-L-alanine in melanin and neuromelanin-containing cells–a possible link between Parkinson-dementia complex and pigmentary retinopathy. *Pigm. Cell Melanoma Res. 22*, 120–130.

(13) Karlsson, O., Lindquist, N. G., Brittebo, E. B., and Roman, E. (2009) Selective brain uptake and behavioral effects of the cyanobacterial toxin BMAA (beta-*N*-methylamino-L-alanine) following neonatal administration to rodents. *Toxicol. Sci. 109*, 286–295.

(14) Karlsson, O., Berg, A.-L., Lindstrom, A.-K., Hanrieder, J., Arnerup, G., Roman, E., Bergquist, J., Lindquist, N. G., Brittebo, E. B., and Andersson, M. (2012) Neonatal Exposure to the Cyanobacterial Toxin BMAA Induces Changes in Protein Expression and Neuro-degeneration in Adult Hippocampus. *Toxicol. Sci. 130*, 391–404.

(15) Karlsson, O., Kultima, K., Wadensten, H., Nilsson, A., Roman, E., Andren, P. E., and Brittebo, E. B. (2013) Neurotoxin-Induced Neuropeptide Perturbations in Striatum of Neonatal Rats. *J. Proteome Res. 12*, 1678–1690.

(16) Karlsson, O., Bergquist, J., and Andersson, M. (2014) Quality Measures of Imaging Mass Spectrometry Aids in Revealing Long-term Striatal Protein Changes Induced by Neonatal Exposure to the Cyanobacterial Toxin beta-N-methylamino-L-alanine (BMAA). *Mol. Cell. Proteomics 13*, 93–104.

(17) Karlsson, O., Berg, A. L., Hanrieder, J., Arnerup, G., Lindstrom, A. K., and Brittebo, E. (2014) Intracellular fibril formation, calcification and enrichment of chaperones, cytoskeletal and intermediate filament proteins in the adult hippocampus CA1 following neonatal exposure to the non-protein amino acid BMAA. *Arch. Toxicol.*, DOI: 10.1007/s00204-014-1262-2, (in press).

(18) Cornett, D. S., Reyzer, M. L., Chaurand, P., and Caprioli, R. M. (2007) MALDI imaging mass spectrometry: molecular snapshots of biochemical systems. *Nat. Methods 4*, 828–833.

(19) Hanrieder, J., Ekegren, T., Andersson, M., and Bergquist, J. (2013) MALDI imaging of post-mortem human spinal cord in amyotrophic lateral sclerosis. *J. Neurochem. 124*, 695–707.

(20) Hanrieder, J., Ljungdahl, A., and Andersson, M. (2012) MALDI imaging mass spectrometry of neuropeptides in Parkinson's disease. *J. Visualized Exp. 60*, e3445.

(21) Passarelli, M. K., and Winograd, N. (2011) Lipid imaging with time-of-flight secondary ion mass spectrometry (ToF-SIMS). *Biochim. Biophys. Acta, Mol. Cell Biol. Lipids 1811*, 976–990.

(22) Lazar, A. N., Bich, C., Panchal, M., Desbenoit, N., Petit, V. W., Touboul, D., Dauphinot, L., Marquer, C., Laprevote, O., Brunelle, A., and Duyckaerts, C. (2013) Time-of-flight secondary ion mass spectrometry (TOF-SIMS) imaging reveals cholesterol overload in the cerebral cortex of Alzheimer disease patients. *Acta Neuropathol. 125*, 133–144.

(23) Hanrieder, J., Phan, N. T. N., Kurczy, M. E., and Ewing, A. G. (2013) Imaging Mass Spectrometry in Neuroscience. *ACS Chem. Neurosci. 4*, 666–679.

(24) Hanrieder, J., Malmberg, P., Lindberg, O. R., Fletcher, J. S., and Ewing, A. G. (2013) Time-of-flight secondary ion mass spectrometry based molecular histology of human spinal cord tissue and motor neurons. *Anal. Chem. 85*, 8741–8748.

(25) Henderson, A., Fletcher, J. S., and Vickerman, J. C. (2009) A comparison of PCA and MAF for ToF-SIMS image interpretation. *Surf. Interface Anal. 41*, 666–674.

(26) Karlsson, O., Roman, E., and Brittebo, E. B. (2009) Long-term cognitive impairments in adult rats treated neonatally with beta-*N*-Methylamino-L-alanine. *Toxicol. Sci. 112*, 185–195.

(27) Karlsson, O., Roman, E., Berg, A. L., and Brittebo, E. B. (2011) Early hippocampal cell death, and late learning and memory deficits in rats exposed to the environmental toxin BMAA (beta-*N*-methylamino-L-alanine) during the neonatal period. *Behav. Brain Res. 219*, 310–320.

(28) Neprasova, H., Anderova, M., Petrik, D., Vargova, L., Kubinova, S., Chvatal, A., and Sykova, E. (2007) High extracellular K(+) evokes changes in voltage-dependent K^+ and Na^+ currents and volume regulation in astrocytes. *Pfluegers Arch. 453*, 839–849.

(29) Farina, C., Aloisi, F., and Meinl, E. (2007) Astrocytes are active players in cerebral innate immunity. *Trends Immunol. 28*, 138–145.

(30) Paxinos, G., and Watson, C. (2007) *The rat brain in stereotaxic coordinates*, 6th ed., Academic Press, Oxford.

(31) Sodhi, R. N. S. (2004) Time-of-flight secondary ion mass spectrometry (TOF-SIMS): Versatility in chemical and imaging surface analysis. *Analyst 129*, 483–487.

(32) Bylesjö, M., Rantalainen, M., Cloarec, O., Nicholson, J. K., Holmes, E., and Trygg, J. (2007) OPLS discriminant analysis: combining the strengths of PLS-DA and SIMCA classification. *J. Chemom. 20*, 341–351.